Hindawi
Journal of Nanomaterials
Volume 2022, Article ID 3342449, 10 pages
https://doi.org/10.1155/2022/3342449

Research Article

The Latest Technology of Polycrystalline Ferroelectric Composite Materials in the Design of the Shovel Frame Structure of the Vibratory Excavating Shovel of the Harvester

Lei Hao and Yanliang Jie

College of Mechanical and Electrical Engineering, Xi'an Traffic Engineering Institute, Xi'an, 710300 Shaanxi, China

Correspondence should be addressed to Lei Hao; haolei@xjy.edu.cn

Received 3 March 2022; Revised 26 April 2022; Accepted 11 May 2022; Published 11 June 2022

Academic Editor: Awais Ahmed

China is a large agricultural country. With the development of industrial production, mechanized harvesting has become an inevitable development trend of agricultural material harvesting. In this paper, based on the latest technology of polycrystalline ferroelectric composite materials in the design of the shovel frame of the harvester's vibrating excavating shovel, the relevant theories of the polycrystalline ferroelectric composite material and the shovel frame of the harvester's vibrating excavating shovel are based on the literature. After understanding, the shovel frame structure of the vibrating excavating shovel of the harvester was designed, and the latest technology of polycrystalline ferroelectric composite material was introduced in the design of the shovel frame of the vibrating excavating shovel of the harvester to make the vibration system have better performance. The designed shovel frame structure is tested, and the test results show that the horizontal output force received by the shovel designed in this paper increases with the increase of speed and is minimized at 0.26 m/s. The vertical output force decreases first and then increases with the increase of speed. It is the smallest when the running speed is 0.39 m/s. The horizontal working resistance is always greater than the vertical working resistance, and it can be seen that the design of the shovel frame structure can be realized in actual work.

1. Inductions

Nowadays, because China's grain crop harvesting work is still labor-based and the level of mechanization of crop production is relatively low, a large amount of labor intensity, labor, and time plus huge costs have significantly reduced agricultural output. Production has had a great negative impact [1, 2]. At present, although some places have adopted mechanical harvesting of crops, they are only used for trenching, and engineers are required to participate in excavation, harvesting, and installation at the same time. Therefore, the degree of mechanization is relatively low. So, harvesting must be mechanized to increase labor efficiency and reduce labor intensity [3, 4].

In the harvester, the vibration function of the harvester is also the main part of the harvester's work. The vibration equipment is also the basic equipment for harvesting. Its structure and motion parameters have a significant impact on the crop damage rate and the labor intensity of manual drilling [5, 6]. Therefore, optimizing and improving the performance of the shock absorber are very important for improving the working efficiency of the harvester.

Aiming at the research on the vibrating shovel of the harvester, some researchers have developed a cassava harvester with a drilling excavator with a built-in main knife structure. The principle is that the main knife penetrates the bottom of the tuber to completely separate the potato soil during harvest. The combine harvester includes harvesting tools, tuber cleaning/traction device, and collector/combiner. In addition to the lifting/loading device, it also has a device to loosen the soil around the cassava tubers, pull the tubers smoothly off the ground, and then use the device to load them onto the truck. Compared with previous harvesters, an advanced feature of this type of machine is the

integration of conveyor and harvester from separation to loading. However, the research on excavation parts and vibrating screens is still in the preliminary test stage, and the relevant research theories are not yet mature. Most cassava harvesters cannot carry out fully mechanized harvesting operations, and more research work is required to use the machines, especially the subsequent finishing operations. In addition, due to different geography and planting conditions, these machines are not completely suitable for cassava harvesting in our country. For this reason, it is necessary to develop a cassava harvester suitable for China's production conditions in accordance with the actual development of cassava in China [7]. Some researchers also pointed out that among the various combined harvesters produced at home and abroad, the excavator screen excavator is particularly suitable for peanut harvesting and film waste collection operations in China. It has the advantages of a low fruit drop rate, the recovery of residual film, the whole film, and the above-ground/underground broken film that can be recovered at the same time, and the recovery rate of residual film is high. However, the traditional single-screen excavator has problems such as large vibration and low soil cleaning effect. In recent years, China has invested a lot of manpower, material, and financial resources in the research and development of film waste-recycling machines, but the current film waste-recycling machines on the market have a single function and low economic performance and commercial value. These are all factors restricting the development of agricultural mechanization in China [8]. Some scholars believe that the excavation and harvesting of most agricultural products have gone through three main stages: shoveling, farming, and mechanical harvesting. Nowadays, the most developed countries have achieved almost mechanized harvesting, but in economically underdeveloped areas, manual harvesting is still the main harvesting method. Digging harvesters generally include digging, soil separation, placement (or collection), and other processes. Among them, excavation equipment and separation and transportation equipment are important components that determine the quality of excavation and harvesting [9]. In the study of polycrystalline ferroelectric composite materials, relevant researchers pointed out the characteristics of polycrystalline ferroelectric composite materials [10]: ferroelectric materials have strong spontaneous polarization, and the iron-based material of the bismuth layer has a high Curie working temperature. In the inspection of the entire bismuth ferroelectric layer material, it does not involve the extraction of the bismuth oxide layer produced by the B-based iron material, the lanthanide A site, and the relaxation type, and the high Curie of most bismuth layer iron materials' working temperature is above 500. At the same time, the ferroelectric material with the bismuth layer has good temperature stability in terms of high dielectric and piezoelectric properties, and the ferroelectric material with the bismuth layer also has an ultrahigh mechanical quality coefficient that reduces the dielectric constant and dielectric loss (2000-7200). Because of the high nonpolarization and low insulation effect of the bismuth oxide layer, the iron-bonded bismuth layer material also has an ultrahigh temperature coefficient of resistivity. This is due to the role of the bismuth peroxide layer in the defect, which makes the perovskite layer more stable, so the contour structure of the bismuth layer ferroelectric material has better fatigue resistance [11]. Other researchers pointed out that multi-iron composites are materials that combine two or more custom-made iron materials in different ways. Among them, composite magnetic electrical materials are a hot research topic. Compared with single-phase magnetic materials, composite magnetic materials have a higher magnetic coupling coefficient, and the temperature of the Curie ferroelectrics and ferromagnets is much higher than at room temperature. Because of these advantages, composite magnetoelectric materials have been extensively studied [12]. In summary, with the development of mechanized production, more and more people begin to pay attention to the design of harvesters, but most of them stay in the theoretical part, and the mechanical applications of the design are not extensive.

This paper studies the shovel frame structure of the vibrating excavating shovel of the harvester, which is the latest technology of polycrystalline ferroelectric composite materials, and analyzes the characteristics of the polycrystalline ferroelectric composite material and the shovel frame structure of the vibrating excavating shovel of the harvester on the basis of literature data. We prepare the theoretical foundation for the following structural design, then design the shovel frame of the harvester's vibrating excavating shovel on the basis of these theories, test the designed structure, and draw relevant conclusions through the test results.

2. Shovel Frame Structure of the Polycrystalline Ferroelectric Composite Material and the Vibrating Shovel of the Harvester

2.1. Characteristics of Polycrystalline Ferroelectric Composite Materials. In addition to the macroscopic characteristics of the electrical group, iron materials have two important characteristics: the structure of the electrical domain and the Curie temperature.

(1) Electric domains refer to small regions with the same spontaneous polarization direction of ferroelectric materials. The boundaries between electrical regions are called domain walls [13]. If the angle between the polarization directions of adjacent electrical regions is 180°, then this region is called a field 180°. If the angle between the polarization directions of adjacent electrical regions is 90°, it is called a field of 90°, as shown in Figure 1. The electric field can be reversed under the action of external force and electric field. This is called electric field change. Applying an electric field opposite to the direction of spontaneous polarization to a ferroelectric substance can reverse the sector by up to 180°, but applying a compressed voltage or a voltage parallel to the direction of spontaneous polarization can reverse the sector by 90°

(2) The spontaneous polarization phenomenon of ferroelectrics only exists in a specific temperature range,

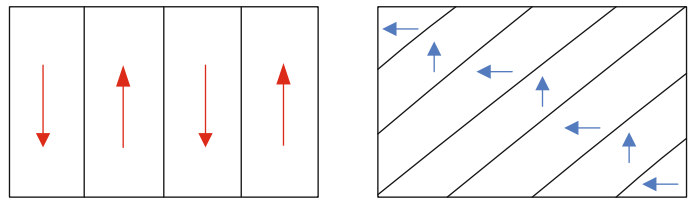

Figure 1: Schematic diagram of domain structure.

and the spontaneous polarization disappears if the temperature exceeds a certain temperature. The ferroelectric has undergone a phase change process from the ferroelectric phase to the normal dielectric phase [14]. That is, the temperature of the corresponding ferroelectric phase transition is called the Curie Tc temperature. Near the Curie temperature, ferroelectrics have many properties, such as dielectric response, piezoelectric response, and pyroelectric effect. Therefore, the Curie temperature change is one of the important means to adjust the physical properties of ferroelectrics

2.2. Application of Polycrystalline Ferroelectric Composite Materials

(1) Research on iron scale effect: due to the development of the thin iron film and ultrafine iron powder technology, the phenomenon of iron size has become a practical problem, so it must be studied in depth in time. Humans first theoretically predicted the changes of spontaneous polarization, phase transition temperature, and dielectric sensitivity of materials with time scales and measured the critical electric strength of typical ferroelectrics [15]. The above results have not only led to the design of a large number of integrated steel electrical components and thin composite materials but also promoted the development of modern polycrystalline ferroelectric composite material theory under limited time scale conditions

(2) Basic research and application research on ferroelectric liquid crystals and ferroelectric polymers: studies have confirmed that the liquid crystals in the inclined laminar flow phase composed of iron chiral atoms have ferroelectricity. In terms of performance, ferroelectric liquid crystals are very advantageous in electrooptical display and nonlinear optical applications. The electrooptical display is mainly through the reversal of polarized light, and its speed is several orders of magnitude higher than that of ordinary filamentary liquid crystal [16]. For nonlinear optics, the effect of second or high-frequency harmonic output exceeds the usual inorganic constitutive nonlinear optics application crystals. Ferropolymers were only recognized more than ten years ago and have a long history with thermoelectrics and piezoelectrics [17]. However, some new types of ferroelectric polymers did not appear until ten years ago. After research, the iron polymer discovered has a wider range of compositions and different structures, so more ferroelectrics appeared later, which expanded the research field of ferroelectric physics and developed new applications

(3) Research on integrated ferroelectrics: the combination of the thin iron film and semiconductor is called integrated ferroelectric, and the research on this material is very extensive [18]. The basic form of ferroelectric memory is random access ferroelectric memory. It was initially considered to be the main purpose of research, and it was not commercialized until 2000 [19]. Compared with the 1950s and 1960s, modern materials and technologies have solved some important problems. First, the use of thin films helps to reduce the depolarization voltage and integrate with standard silicon or circuits, and the fatigue performance is significantly improved, resulting in multiple inverted iron films, which have gradually realized important uses in memory. At the same time, the application of ferroelectric thin films is not limited to the storage field but also includes ferroelectric effect transistors and ferroelectric random access memories. In addition to memory, the built-in ferroelectrics can also be used in infrared detection and imaging equipment, ultrasonic and surface acoustic equipment, and optoelectronic equipment. It can be seen that the built-in thin film devices have huge application prospects

2.3. The Shovel Frame Structure of the Vibratory Excavating Shovel of the Harvester

2.3.1. Working Principle of Harvester. As shown in Figure 2, the excavator operation process has typical cyclic characteristics, whether it is a front excavator or a reverse excavator drilling method. The cycle process mainly includes five stages: drilling, emptying the bucket, rotating, unloading, and drilling. The important stage of drilling design energy consumption is also the stage when the working device is subjected to drastic random load changes. During the entire drilling phase, very complex physical and mechanical phenomena occur between the bucket and the soil, that is, the soil is destroyed. The bucket is the first tangent to the ground at a specific initial speed and cutting force. If it is a forward drilling method, the main purpose is to destroy the integrity of the accumulated soil. After being completely destroyed, gravity causes the soil to roll into the shovel. At

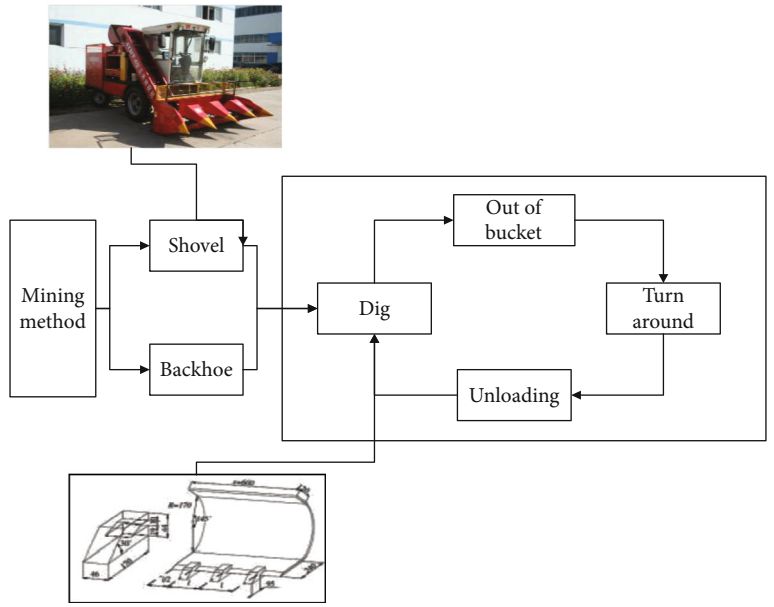

Figure 2: Working principle of the harvester.

the same time, the bucket continues to cut deeply until the bucket is full. This mode of operation mainly occurs in open-pit mining and mineral blasting. The main purpose of excavator drilling is to destroy the soil structure.

2.3.2. The Relevant Parameters of the Shovel Frame of the Vibratory Excavating Shovel of the Harvester

(1) The Surface Inclination of the Vibrating Shovel of the Harvester. The vibrating shovel is also one of the main parts of the digging harvester, which directly affects the efficiency of the whole machine, and the shovel surface angle a is the main reason that affects the quality of the excavator [20]. Inappropriate viewing angles can cause soil retention and increase operating power. The design principle of angle a is to make the excavated material rise to a certain height along the surface of the bucket machine to prevent the excavated material from falling in the middle direction. At the same time, the excavation object should also do the following: the excavation is smooth, and it is transferred to the rear vibrating screen to gradually eliminate soil dirt.

According to design experience, if the angle a is larger, the crop soil mixture will be scattered on both sides and trapped in the digging shovel. In fact, the angle a is determined by many factors, such as the ability to loosen the soil, the height of the drilling material lifted by the excavator, and the characteristics of the soil. The larger the angle a, the weaker the ground, but it also increases the digging resistance and tends to maintain the ground. The smaller the angle a, the smaller the digging resistance of the excavator, the better the ground, and the higher the penetration efficiency, but the crushing effect of the shovel on the ground is reduced. At $a = 25^{\circ}$, the moderately hard sandy loam is obviously blocked. So, in summary, the inclination value of the shovel surface is initially set in the range of 18°-26°.

2.3.3. Vibration Drive Device. The drive unit is mainly used to drive vibration. The drive unit is mainly composed of a drive shaft, a front-drive joint, a rear-drive joint, a cam-drive arm, and a cam block. The transmission structure transmits power from the power output shaft of the tractor to the drive shaft. The drive shaft drives the cam to reciprocate. The front-drive connector and the rear-drive connector move forward and backward at the same time under the influence of the eccentric drive arm during driving [21].

The design of the drive camshaft arm is mainly used for the reverse movement of the two vibrating rods. The mass of the eccentric transmission vibrating arm is 2.67 kg, the eccentricity is 9 mm analyzed by the 3D software center of gravity analysis unit, and the calculated moment of inertia is 0.024 kg m. When the eccentric drive arm rotates, the inertial force will be generated, which will cause the whole machine to vibrate and affect the stability and service life of the machine tool. Therefore, it is necessary to balance the vibration. Therefore, it is necessary to install an eccentric mass with the moment of inertia such as an eccentric drive arm on the drive shaft. The mass is 1.78 kg, and the eccentricity (the distance from the center of the camshaft to the drive shaft) is 13.5 nm. The eccentric block of the eccentric transmission arm and the camshaft are symmetrical about the axis of the transmission shaft and are both located on the transmission shaft to neutralize the moment of inertia generated during operation.

2.4. Related Calculation Model. The discrete element method (DEM) is a numerical simulation method for calculating complex discrete systems, mainly used to calculate the mechanical and kinematic properties of granular materials [22]. When analyzing mechanical problems, many mechanical or motion systems are usually involved. The laws and states of each system can be expressed and calculated through the interaction of mathematical analysis functions.

For the more complicated problems when using this mathematical analytical function method, new arithmetic methods have emerged, such as the finite element method (FEM) and the discrete element method. The finite element method divides the system to be analyzed into microscopic units, approximates each unit with a simple mathematical analysis function with limited degrees of freedom, and calculates the increase of the entire system through each microscopic unit. Similar to the idea of the finite element method, the discrete element method treats the entire system as a collection of interacting discrete units, analyzes the interaction between the discrete units, and then combines the mechanical action and exchange of energy between the units to obtain the analysis results of the entire discrete system and the mechanical influence on the external structure [23].

In summary, this paper uses the Hertz-Mindlin model to carry out discrete element numerical simulation experiments [24]. Suppose there are two spheres with radii of R_1 and R_2, and δ_n is the amount of normal overlap:

$$\delta_n = R_1 + R_2 - \left|\vec{r}_1 - \vec{r}_2\right|, \tag{1}$$

where $\vec{r}_1$ and $\vec{r}_2$ are the vector positions of the centroids of the two particles.

Then the size of the contact radius a is equal to

$$a = \sqrt{\delta_n R^*}. \tag{2}$$

In the formula, R^* is the equivalent radius of the particle, and the derivation formula is as follows:

$$\frac{1}{R^*} = \frac{1}{R_1} + \frac{1}{R_2}. \tag{3}$$

The normal phase force between particles F_n is

$$F_n = \frac{4}{3}E^*(R)^{1/2}{\delta_n}^{3/2}, \tag{4}$$

$$\frac{1}{E^*} = \frac{1-{\lambda_1}^2}{E_1} + \frac{1-{\lambda_2}^2}{E_2}, \tag{5}$$

where E^* is the equivalent elastic modulus between particles, E_1 and E_2 are the elastic modulus of two spherical particles, respectively, and λ_1 and λ_2 are the Poisson's ratio.

The normal damping force calculation formula is

$$F_n^d = -2\sqrt{\frac{5}{6}}\beta\sqrt{S_n m^*}\,v_n^{rel}, \tag{6}$$

$$m^* = \frac{m_1 m_2}{m_1 + m_2}, \tag{7}$$

$$v_n^{rel} = \left(\vec{v}_1 + \vec{v}_2\right) \times \vec{n}. \tag{8}$$

Among them, m^* is the mass equivalent, m_1, m_2 is the mass of the two particles, and v_n^{rel} is the relative velocity of the normal phase between the two particles.

The calculation formula of the tangential force between particles is

$$F_t = -S_t d_t, \tag{9}$$

$$S_t = 8G^*\sqrt{R^*\alpha}, \tag{10}$$

$$G^* = \frac{2-{\nu_1}^2}{G_1} + \frac{2-{\nu_2}^2}{G_2}, \tag{11}$$

where G^* is the gravitational velocity.

The calculation formula of tangential damping force is

$$F_t^d = -2\sqrt{\frac{5}{6}}\beta\sqrt{S_t m^* v_t^{rel}}. \tag{12}$$

In the formula, v_t^{rel} is the tangential relative velocity between the two particles.

3. The Shovel Frame Structure Design of the Vibratory Excavating Shovel of the Harvester

3.1. Application of the Latest Technology of Polycrystalline Ferroelectric Composite Materials. The shovel frame structure of the excavating shovel of the harvester should be applied to the ferroelectricity of the polycrystalline ferroelectric composite material to realize good control of the shovel frame structure. This article expands the application of the polycrystalline ferroelectric composite material in the vibration system.

3.1.1. Principle of Vibration System. The excavator designed in this research adopts the principle of vibration. When the vibrating excavator is working, the control unit adopts a pulse generator (motor, rotary valve). The structure of the oil circuit of the vibrating cylinder retracts the piston rod of the vibrating cylinder, and the shovel mounted on the piston rod vibrates and destroys the soil. Since the shovel returns through the return spring, it can drive the shovel to vibrate back and forth in a balanced position [24].

3.1.2. Vibration Structure. The vibrating shovel is driven by a ZL50G loader and provides a hydraulic drive. The hydraulic system of the vibrating excavator is powered by a gear pump connected in series with the main pump of the loader ZL50G. The gear pump drives four parallel vibrating oil cylinders to move, and the excavating shovel moves under each vibrating oil cylinder. The vibrating cylinder periodically provides active vibration, and the return spring provides a specific pressure to reset the shovel [25]. The excavating shovel is made of a 65Mn steel plate and is fixed on the component with bolts, which can be easily replaced after wear.

Based on the above analysis, the control during the vibration process is very critical. Therefore, in order to have a better control capability of the vibration system, an integrated ferroelectric is used to design the system circuit.

3.2. Design of the Opening Angle of the Shovel Surface of the Shovel. The design of the opening angle of the drilling shovel directly affects the resistance of the drilling. If the opening

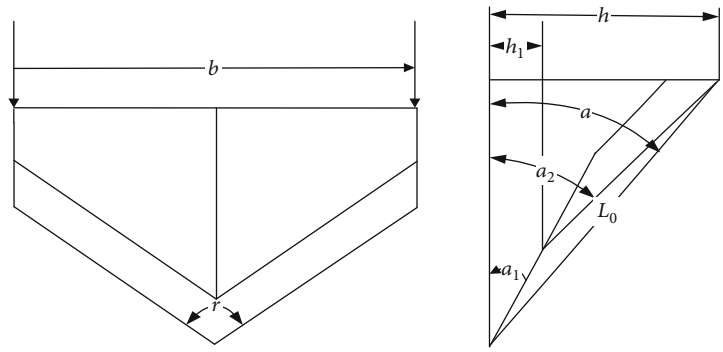

Figure 3: Geometry diagram of the blade edge.

angle of the digging shovel surface is too large, the stems, leaves, and weeds are not easy to be cut during the operation of the digging shovel, and the movement resistance is large, which will increase the power consumption of the machine and increase the manufacturing cost [26]. Therefore, it is necessary to adjust the opening angle r of the digging shovel blade so that the stems, leaves, and weeds can slide smoothly along the edge of the shovel blade to reduce the digging resistance.

In the structural design of the second-order curved shovel, the opening angle of the shovel surface directly affects the digging resistance of the shovel surface during excavation. If the opening angle of the shovel surface is too large, the shovel blade will be difficult to cut stems, leaves, and weeds and will be easily tangled, resulting in a sharp increase in drilling resistance and increased energy consumption. Therefore, it is necessary to effectively control the opening angle of the shovel surface. To achieve the purpose of cutting stems, leaves, and weeds, reduce the resistance to drilling. According to the geometric relationship shown in Figure 3, the total resistance p of the stem, weeds, and soil at the end of the leaf is decomposed along the direction of the leaf and perpendicular to the direction of the leaf. The geometric relationship is as follows:

3.2.1. Design of Inclination Angle of Shovel. In order to study the change law of convex curved shovel resistance with the inclination of the shovel face and the length of the shovel body, the virtual shovel face inclination is introduced into the resistance calculation formula to realize the approximate calculation of the curved shovel. When the virtual shovel surface inclination and the length of the shovel body are unknown quantities, the calculation results are shown in Figure 4.

The comprehensive analysis in Figure 4 shows that under various combinations of the virtual shovel surface length and the subsurface inclination angle, the drilling resistance increases with the increase of the drilling depth. In addition, the length of the virtual surface of the shovel also has a certain influence on the resistance of the shovel. Under the same combination of digging shovel surface inclination angle, as the virtual length of digging shovel surface increases, the digging resistance tends to decrease, but the effect is not significant. In the actual design, the surface length of the excavating shovel should not be too long; otherwise, the soil-blocking phenomenon will be more serious when harvesting crops. On the other hand, it is unfavorable for the soil separation of the next vibrating device, and the load capacity of the tool alone is increased to increase the power consumption.

In order to study the variation of convex curved shovel resistance with the height of the shovel surface, the virtual shovel surface height is introduced into the resistance calculation formula to realize the approximate calculation of the curved shovel. When the virtual shovel surface height is an unknown quantity, the calculation results are shown in Figure 5.

The analysis of the change curve of top resistance with the height of the primary shovel (Figure 5) shows that the resistance of the shovel decreases with the increase of the height of the primary shovel. It can be seen that the height of the stepped excavating shovel has a great influence on the excavation resistance. Therefore, when designing the excavating shovel, the height of the stepping excavating shovel must be appropriately selected so that the digging resistance will not become too high. The resistance of the shovel is also closely related to the combination of shovel inclination. Analyzing Figure 5, it can be seen that even if the slope of the main shovel changes, the slope of the auxiliary shovel will not change. When the shovel resistance changes and the inclination of the front surface of the main shovel is determined, if the inclination of the auxiliary shovel surface increases, the resistance of the shovel surface increases sharply. Therefore, the change of the inclination angle of the secondary excavator has a great influence on the resistance, and it is more obvious. The difference in the inclination angle of the two steps can be used to measure the crushing ability of the surface of the secondary excavating shovel. The greater the difference, the higher the crushing capacity, but the greater the surface resistance of the shovel.

After analyzing and studying the relationship between the inclination angle of the secondary surface curve and the drilling resistance, it may be found that the inclination angle of the main excavator surface must be smaller than the secondary inclination angle, and the difference between the two inclination angles cannot be too large or too small. If the value is too high, if the surface soil compressibility of

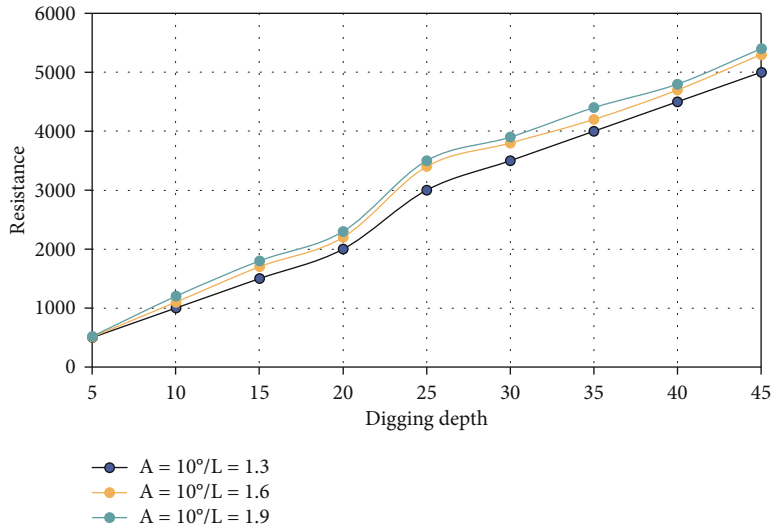

Figure 4: The relationship curve between digging depth and resistance when combined with different inclination angles.

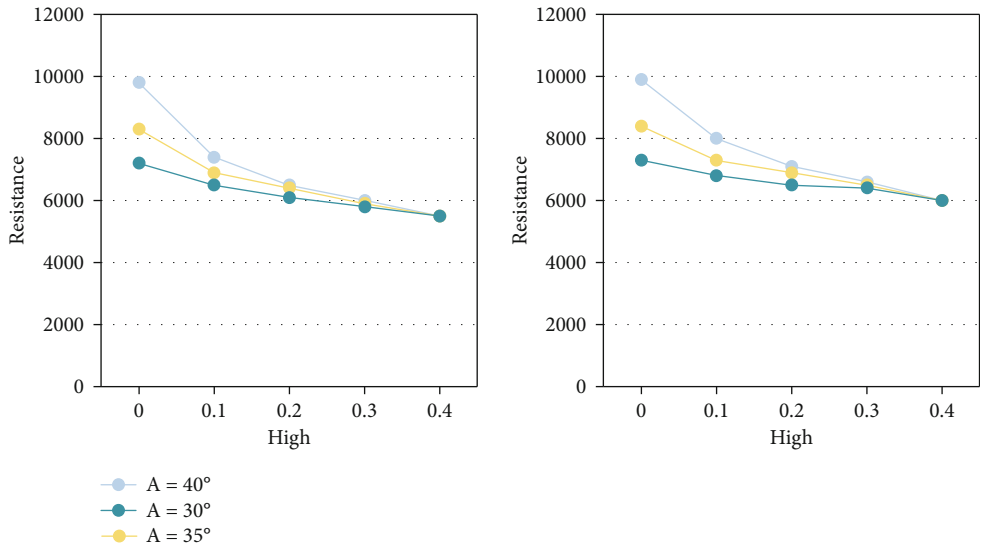

Figure 5: Change curve with the height of the primary excavating shovel.

the digging shovel is low, the surface resistance of the digging shovel will increase sharply. If the value is too low, the soil will not have enough compressibility, but the resistance will be relatively low. Based on the above situation, the combined inclination angle of the convex surface of the excavating shovel pair is 15° and 30°.

3.3. Shovel Body Length Design. The length design of the shovel body should follow this principle. The length of the shovel body cannot be too long or too small. The length of the shovel body of the digging shovel is so long that the resistance between the soil body and the shovel surface is very small. However, when harvesting, the rear edge of the digging shovel surface is seriously blocked, which makes the crop fragile and affects the harvesting effect. The length of the shovel body is too small to cause the crops to be brought to the vibration chain of the conveyor before breaking, it is also difficult to break due to vibration, and the energy consumption of the vibration chain of the conveyor increases sharply. Therefore, the length design of the shovel

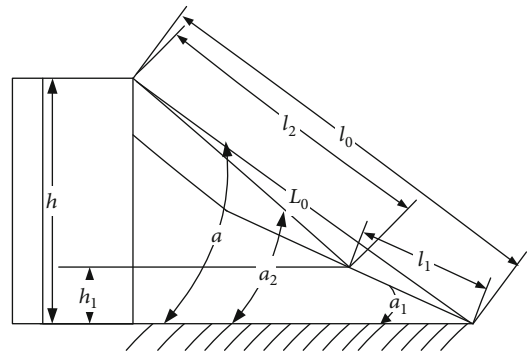

Figure 6: Schematic diagram of the length of the shovel body.

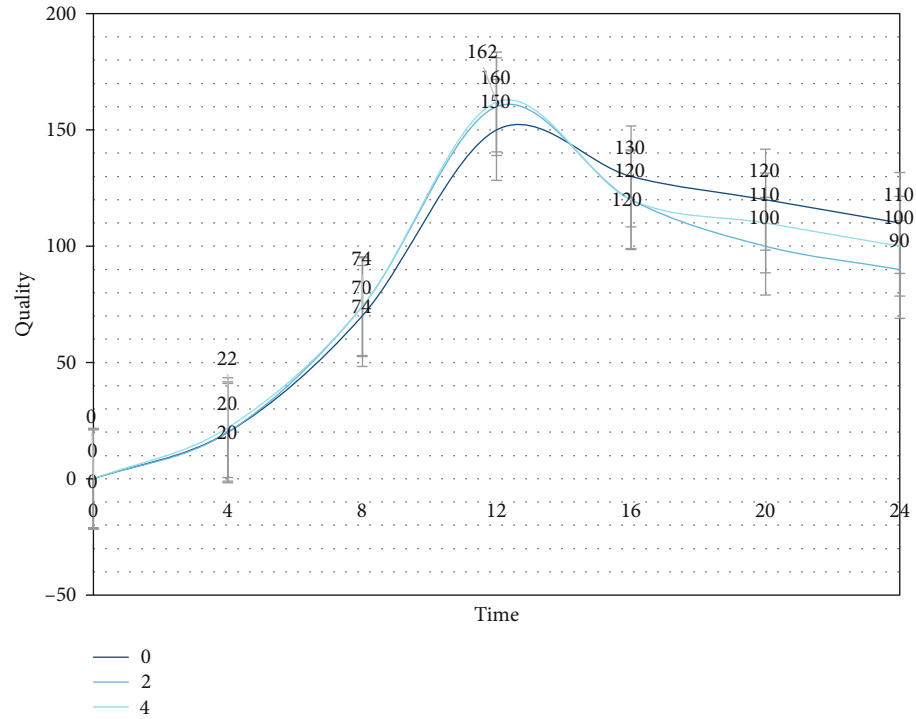

Figure 7: The bucket material quality change curve with time.

body should comprehensively consider the above factors and carry out a reasonable design.

The length of the shovel body is determined as shown in Figure 6, l_0 is the virtual shovel face length, l_1 is the first shovel face length, l_2 is the second shovel face length, a is the virtual shovel face inclination, a_1 is the first shovel face inclination, a_2 is the inclination angle of the second-stage shovel surface, h is the height of the rear end of the shovel body, and h_1 is the height of the first-stage shovel surface.

The actual design of the shovel body length should ensure that the speed is not zero when moving to the rear end of the first section; otherwise, the soil cannot be transported in time, causing a blockage.

3.4. Design of the Number of Teeth. For the bucket model for three different numbers of teeth (the number of teeth is 0, 2, and 4), a three-dimensional numerical model of the natural accumulation of noncohesive minerals during bucket drilling was established, the bucket manipulation process was visualized, and the bucket load during the entire drilling period was extracted. Compared with the previous model test and overall test method, the numerical simulation method guarantees the consistency of the test to a large extent, avoids the reproducibility and reproducibility of the model test, improves the reliability of the results, and reduces the influencing factors. The test cost and test cycle are reduced [27]. The experimental results are processed, and three types of hopper material quality curves that change with time (Figure 7) are extracted to explain the filling information and flow of the hopper material.

Through the processing of the test results, as shown in Figure 7, three types of bucket material quality changes that change over time are extracted, and the filling information and flow of the materials in the bucket are described. The figure shows that the quality curves of the three buckets tend to be the same but have different widths and different final constant values. From 0 to 15 seconds, the quality of the three buckets will be significantly improved. Within 0-4 seconds, the gradient becomes smaller, indicating that the integrity of the material has been destroyed by the bucket teeth, and it begins to flow into the bucket. Starting from 4 seconds, the slope of the curve increases sharply. Large means that the material starts to enter the bucket quickly in large quantities. The slopes of the three curves are similar, but due to the difference in the number of bucket teeth, the quality of the bucket begins to vary. This difference is maximized in 6 seconds. The mass of the four-tooth bucket is

Table 1: Discrete element simulation parameters.

Parameter	Numerical value
Soil particle radius (m)	0.001~0.003
Number of simulated soil particles	400000
Soil density (kg/m^2)	1540
Soil Poisson's ratio	0.3
Soil shear modulus (Pa)	$1.01e+06$
Digging shovel density (kg/m$'$)	7890
Poisson's ratio of digging shovel	0.269
Shear modulus of shovel (Pa)	$8.2e+10$
Time step (s)	$2.65e-05$
Total simulation time (s)	52~53

Table 2: Discrete element simulation results 1.

Working speed (m/s)	Horizontal force of the shovel (N)	Vertical force of the shovel (N)
0.26 m/s	55.91	55.65
0.37 m/s	62.21	47.89
0.48 m/s	66.12	52.34

Table 3: Discrete element simulation results 2.

Working speed (m/s)	Horizontal force of the shovel (N)	Vertical force of the shovel (N)
0.26 m/s	55.91	55.65
0.39 m/s	66.99	44.21
0.52 m/s	89.43	59.76

Table 4: Discrete element simulation results 3.

Working speed (m/s)	Horizontal force of the shovel (N)	Vertical force of the shovel (N)
0.35 m/s	55.81	55.52
0.37 m/s	66.99	44.89
0.39 m/s	89.43	59.76

43.40 tons. Compared with the teeth in bucket 0, the mass of the 2,964-ton bucket is almost 46.4% higher.

Observe the change of each curve from the maximum mass of the entire bucket to the final speed. The less the number of bucket teeth, the more stable the quality of the bucket and full bucket, that is, the more stable the maximum mass and final speed. The fewer the number of teeth, the lower the quality of the spilled material when the material quality in the bucket is maximized. Therefore, from the test results, it may be a reasonable choice to place less or no teeth on the nonsticky drilling material.

4. The Shovel Frame Structure Test of the Vibrating Excavating Shovel of the Harvester

In this chapter, using the EDEM discrete element modeling software, according to the physical and mechanical parameters of the soil, a soil particle model was established, combined with field test conditions, and a 3D model of the harvester for simulation adjustment was created. A particle factory will be built to simulate the work of the harvester. The movement of the ground and the power of the shovel were observed in the process. The harvester uses discrete data methods to simulate working resistance at six different operating speeds (0.26 m/s, 0.35 m/s, 0.37 m/s, 0.39 m/s, 0.48 m/s, and 0.52 m/s). A discrete data method is used to study the feasibility of harvester, and a new digital design research method is provided for this.

4.1. Establishment of Discrete Element Model. Use the EDEM software to simulate and analyze the working resistance of the harvester. In addition to obtaining the physical and material parameters of the soil and harvester in advance, it is also necessary to select the correct contact model and create a soil particle model. Create geometry for the shovel model, set limits for the simulation area, create a particle factory, and run the simulation.

4.2. Selection of Discrete Element Simulation Parameters. The closeness of the discrete simulation results to the actual field test results mainly depends on the choice of discrete simulation parameters. The selection of parameters is to consult relevant documents and make adjustments according to the simulation process. The specific simulation parameter values are shown in Table 1.

4.3. Discrete Element Simulation Results and Analysis. The simulation test adopts a single-factor test, which only changes the forward speed of the excavating shovel along the negative direction of the X-axis. The forward speed of the excavating shovel is adjusted in the six simulation tests. The negative direction along the X-axis is 0.26 m/s, 0.35 m/s, 0.37 m/s, 0.39 m/s, 0.48 m/s, and 0.52 m/s, respectively. The simulation results are divided into three groups. The specific data results are shown in Tables 2–4.

Analyzing the above simulation test data table, if other simulation parameters are consistent, changing the forward speed of the excavating shovel in the negative direction of the X-axis increases with the increase of the horizontal force of the excavating shovel. The increase first decreases and then increases. The working speed is 0.39 m/s, and the horizontal working resistance is always greater than the vertical working resistance.

5. Conclusions

This paper studies the shovel frame structure of the vibratory excavating shovel of the harvester with the latest technology of polycrystalline ferroelectric composite materials. After understanding the relevant theories, the shovel frame structure of the vibrating excavating shovel of the harvester is designed. In the shovel frame structure, the latest technology of polycrystalline ferroelectric composite material is introduced to make the vibration system have better performance, and the designed shovel frame structure is tested through actual tests. The test result shows that when the minimum speed is 0.26, the vertical resultant force first decreases and then increases with the increase of speed. The operating speed is 0.39 m/s, and the horizontal operating resistance is always greater than the vertical operating resistance. Therefore, the shovel frame structure designed in this paper is feasible in actual work. However, there are still some shortcomings in the research process of this article, which are mainly manifested in the absence of an actual field experiment.

Data Availability

No data were used to support this study.

Conflicts of Interest

The authors declare that there are no conflicts of interest regarding the publication of this article.

References

[1] Y. Dong, M. J. Hossain, and J. Cheng, "Performance of wireless powered amplify and forward relaying over Nakagami- fading channels with nonlinear energy harvester," *IEEE Communications Letters*, vol. 20, no. 4, pp. 672–675, 2016.

[2] G. Litak, M. I. Friswell, and S. Adhikari, "Regular and chaotic vibration in a piezoelectric energy harvester," *Meccanica*, vol. 51, no. 5, pp. 1017–1025, 2016.

[3] P. S. Mederski, M. Bembenek, Z. Karaszewski, A. Łacka, A. Szczepańska-Álvarez, and M. Rosińska, "Estimating and modelling harvester productivity in pine stands of different ages, densities and thinning intensities," *Croatian Journal of Forest Engineering*, vol. 37, no. 1, pp. 27–36, 2016.

[4] Y. Wang, W. Liang, T. Cheng, Z. Song, and F. Qin, "Sealed piezoelectric energy harvester driven by hyperbaric air load," *Applied Physics Letters*, vol. 108, no. 3, p. 33902, 2016.

[5] S. P. S. Guerra, G. Oguri, and R. Spinelli, "Harvesting eucalyptus energy plantations in Brazil with a modified New Holland forage harvester," *Biomass & Bioenergy*, vol. 86, no. Mar., pp. 21–27, 2016.

[6] Z. Hameed and K. Moez, "A 3.2 V −15 dBm adaptive threshold-voltage compensated RF energy harvester in 130 nm CMOS," *IEEE Transactions on Circuits & Systems I Regular Papers*, vol. 62, no. 4, pp. 948–956, 2015.

[7] R. Hosseini and M. Hamedi, "An investigation into resonant frequency of trapezoidal V-shaped cantilever piezoelectric energy harvester," *Microsystem Technologies*, vol. 22, no. 5, pp. 1127–1134, 2016.

[8] L. Q. Chen, W. A. Jiang, M. Panyam, and M. F. Daqaq, "A broadband internally-resonant vibratory energy harvester," *Journal of Vibration & Acoustics*, vol. 138, no. 6, 2016.

[9] Y. Zhang, T. Wang, A. Luo, Y. Hu, X. Li, and F. Wang, "Micro electrostatic energy harvester with both broad bandwidth and high normalized power density," *Applied Energy*, vol. 212, pp. 362–371, 2018.

[10] Y. Zhang, W. Ni, and Y. Li, "Effect of siliconizing temperature on microstructure and phase constitution of Mo-$MoSi_2$ functionally graded materials," *Ceramics International*, vol. 44, no. 10, pp. 11166–11171, 2018.

[11] X. Liu, L. Huang, K. Ravichandran, and E. Sanchez-Sinencio, "A highly efficient reconfigurable charge pump energy harvester with wide harvesting range and two-dimensional MPPT for internet of things," *IEEE Journal of Solid-State Circuits*, vol. 51, no. 5, pp. 1302–1312, 2016.

[12] H. Xiao, X. Wang, and S. John, "A multi-degree of freedom piezoelectric vibration energy harvester with piezoelectric elements inserted between two nearby oscillators," *Mechanical Systems & Signal Processing*, vol. 68, pp. 138–154, 2016.

[13] S. Lemey, S. Agn Ee Ssens, P. V. Torre, K. Baes, J. Vanfleteren, and H. Rogier, "Wearable flexible lightweight modular RFID tag with integrated energy harvester," *IEEE Transactions on Microwave Theory and Techniques*, vol. 64, no. 7, pp. 2304–2314, 2016.

[14] C. K. Jeong, S. B. Cho, J. H. Han et al., "Flexible highly-effective energy harvester via crystallographic and computational control of nanointerfacial morphotropic piezoelectric thin film," *Nano Research*, vol. 10, no. 2, pp. 437–455, 2017.

[15] D. Pan, Y. Li, and F. Dai, "The influence of lay-up design on the performance of bi-stable piezoelectric energy harvester," *Composite Structures*, vol. 161, pp. 227–236, 2017.

[16] P. Li, S. Gao, H. Cai, and L. Wu, "Theoretical analysis and experimental study for nonlinear hybrid piezoelectric and electromagnetic energy harvester," *Microsystem Technologies*, vol. 22, no. 4, pp. 727–739, 2016.

[17] P. Wang, T. Yao, Z. Li et al., "A superhydrophobic/electrothermal synergistically anti-icing strategy based on graphene composite," *Composites Science and Technology*, vol. 198, article 108307, 2020.

[18] G. Bo, L. Chang, H. Chenglong et al., "Effect of mg and RE on the surface properties of hot dipped Zn–23Al–0.3Si coatings," *Science of Advanced Materials*, vol. 11, no. 4, pp. 580–587, 2019.

[19] X. Wang, C. Chen, N. Wang et al., "A frequency and bandwidth tunable piezoelectric vibration energy harvester using multiple nonlinear techniques," *Applied Energy*, vol. 190, pp. 368–375, 2017.

[20] H. C. Song, P. Kumar, D. Maurya et al., "Ultra-low resonant piezoelectric MEMS energy harvester with high power density," *Journal of Microelectromechanical Systems*, vol. 26, no. 6, pp. 1226–1234, 2017.

[21] M. Gao, W. Ping, C. Yong, R. Chen, and D. Cai, "Design and verification of a rail-borne energy harvester for powering wireless sensor networks in the railway industry," *IEEE Transactions on Intelligent Transportation Systems*, vol. 18, no. 99, pp. 1596–1609, 2017.

[22] N. Sharpes, A. Abdelkefi, H. Abdelmoula, P. Kumar, J. Adler, and S. Priya, "Mode shape combination in a two-dimensional vibration energy harvester through mass loading structural modification," *Applied Physics Letters*, vol. 109, no. 3, p. 033901, 2016.

[23] C. Tao, Y. Xia, W. Liu, H. Liu, L. Sun, and C. Lee, "A hybrid flapping-blade wind energy harvester based on vortex shedding effect," *Journal of Microelectromechanical Systems*, vol. 25, no. 5, pp. 845–847, 2016.

[24] J. H. Kim, J. S. Kim, S. H. Han, H. W. Kang, H. G. Lee, and C. I. Cheon, "(K,Na)NbO_3-based ceramics with excess alkali oxide for piezoelectric energy harvester," *Ceramics International*, vol. 42, no. 4, pp. 5226–5230, 2016.

[25] Q. Lu, L. Liu, F. Scarpa, J. Leng, and Y. Liu, "A novel composite multi-layer piezoelectric energy harvester," *Composite Structures*, vol. 201, no. OCT., pp. 121–130, 2018.

[26] K. Adamski, J. Adamski, J. A. Dziuban, and R. Walczak, "Inkjet 3D printed miniature water turbine energy harvester-flow meter for distributed measurement systems," *In Multidisciplinary Digital Publishing Institute Proceedings*, vol. 1, no. 4, pp. 578–578, 2017.

[27] Y. Tan, D. Ying, and X. Wang, "Review of MEMS electromagnetic vibration energy harvester," *Journal of Microelectromechanical Systems*, vol. 26, no. 1, pp. 1–16, 2017.